Magnetic configuration effects on TAE-induced losses and a comparison with the orbit-following model in the Large Helical Device

Magnetic Configuration Effects on TAE-induced Losses

and Comparison with Orbit-Following Model in the LHD

Kunihiro OGAWA, Mitsutaka ISOBE, Kazuo TOI, Donald A. SPONG[1],

Masaki OSAKABE, LHD Experiment Group

National Institute for Fusion Science, 322-6 Oroshi-cho, Toki 509-5292, Japan

[1]*Oak Ridge National Laboratory, Oak Ridge, Tennessee 37831-6169, USA*

email:ogawa.kunihiro@lhd.nifs.ac.jp

Abstract

Fast-ion losses from LHD plasmas due to toroidal Alfvén eigenmodes (TAEs) were measured by a scintillator-based lost fast-ion probe (SLIP) to understand the loss processes. TAE-induced losses measured by the SLIP appeared in the ranges of energy E of around 50~180 keV and pitch angle χ of 35°~45°, and increased with the increase of TAE amplitudes. Position shifts of the magnetic axis due to finite plasma pressure led not only to an increase of TAE-induced losses but also to a stronger scaling of fast-ion losses on TAE amplitudes. Characteristics of the observed fast-ion losses were compared with a

numerical simulation based on orbit-following models in which the TAE fluctuations are taken into account. The calculation indicated that the number of lost fast-ions reaching the SLIP increased with the increase of the TAE amplitude at TAE gap. Moreover, the calculated dependence of fast-ion loss fluxes on the fluctuation amplitude became stronger in the case of large magnetic-axis shifts, compared with the case of smaller shifts, just as was observed in the experiments. The simulation results agreed qualitatively with the experimental observations in LHD.

1. Introduction

For a fusion device such as the ITER, alpha-particle-driven Alfvén eigenmode (AE) instabilities [1] are predicted to induce local damage of the plasma-facing components if the AE causes appreciable loss of fusion-born energetic alpha particles. Studies of fast-ion loss processes in mid- or large-sized tokamaks have been carried out experimentally and theoretically over two decades to investigate ways to control/reduce the fast-ion losses in fusion devices [2-4]. In particular, the scintillator-based lost fast-ion probe (SLIP) has been extensively used as a diagnostic system for understanding the fast-ion loss process [5-7]. The first SLIP was built at Princeton's Tokamak Fusion Test Reactor (TFTR) [8-10]. SLIPs are attractive for their ability to simultaneously measure

the energy and pitch angle of escaping fast ions. SLIPs have played an important role for the study of alpha particle loss due to magnetohydrodynamic (MHD) instabilities as well as due to magnetic-field ripple in tracking the orbits of lost alpha particles at TFTR [11].

Fast-ion transport and/or losses caused by AEs have been regularly observed in fusion plasmas when substantial numbers of super-Alfvénic ions are present. It has been found that various AE modes can induce fast-ion losses [12]. Study of AE-induced fast-ion losses with the aid of numerical simulation is also important to obtain deeper understanding of the physics involved [13]. Recently, an attempt was made to simulate the nonlinear evolution of a single TAE as well as fast-ion losses using a hybrid simulation code for MHD fluid interaction with fast ions [14].

Better understanding of the loss processes can be obtained through the comparison of fast-ion loss data between tokamaks and heliotron/stellarator devices, because AEs having different structures can be excited by different rotational transform profiles [15, 16]. The physics of AEs has been extensively studied in heliotron/stellarator devices. Studies using the SLIP to measure beam-ion losses induced by AEs on medium-scale devices have been published [17, 18]; these were observations of TAE-induced or energetic-particle continuum mode (EPM)-induced losses in the Compact Helical System (CHS) [19] and global Alfvén eigenmode (GAE)-induced loss

in the Wendelstein 7-AS [20]. Recently, beam-ion transport/losses induced by toroidal

Alfvén eigenmodes (TAEs) have also been observed in a large-scale device, namely, the

Large Helical Device (LHD) in Gifu, Japan. In previous works on LHD, the anomalous

radial transport and losses of co-going beam ions due to TAE instabilities have been

observed in plasmas with large Shafranov shifts for LHD configurations that have the

magnetic axis position in the vacuum field at $R_{ax\_vac} = 3.6$ m; these measurements were

made using an $E//B$ neutral particle analyzer with a tangential line of sight [21] and using

a SLIP [15, 22]. Although a great deal of effort has been expended on the measurement of

fast-ion transport and loss due to TAE instabilities in heliotron/stellarator plasmas, further

understanding of the effects of the magnetic configuration on fast-ion losses and fast-ion

loss modeling is required.

This work was conducted to clarify the Shafranov shift effect on fast-ion loss

processes in relatively high beta plasmas with super-Alfvénic beam ions in LHD.

Characteristics of TAE-induced fast-ion losses measured by the SLIP are compared with

those of the fast-ion losses calculated by an orbit-following simulation. In particular, we

focused on a comparison of the scaling of fast-ion loss as a function of TAE amplitudes.

This paper is organized as follows. In section 2, a brief introduction of the experimental

set-up on the LHD is described. Experimental observation of TAE-induced losses is

presented in section 3, together with a detailed analyses of the experimental data. The orbit-following model composed of two orbit codes is described in Sec.4. The characteristics of TAE-induced losses simulated by the orbit-following model are shown in section 5. Section 6 summarizes the work.

2. Experimental setups

2.1 Beam ions

A bird's-eye view of the LHD with negative-ion source-based neutral beam injectors (N-NBI) together with the SLIP is shown in Fig. 1. The LHD is equipped with three tangential N-NBIs, providing injection energies up to 180 keV. One beam injects hydrogen neutral beams in the clockwise direction while the other beams inject them in the counter-clockwise (CCW) direction, as seen from the top. These ions provide a free energy source to destabilize the AEs. Strong TAEs are often destabilized when super-Alfvénic beam ions produced by these neutral beams are present in relatively low-B_t plasmas.

2.2 Diagnostics

The SLIP plays an important role in this work, detecting lost fast-ion flux,

together with the Larmor radius, from which the fast-ion energy can be inferred: namely

$\rho = (2m_h E)^{1/2}/q_h B_{SLIP}$ and $\chi = \arccos(v_{//}/v)$. Here, m_h, q, B_{SLIP} $v_{//}$, and v represent the ion

mass, the electric charge, the magnetic field strength at the SLIP head position, the

velocity of ions parallel to the magnetic field and the velocity of the ions, respectively.

The SLIP is placed at major radius $R = 4.62$ m, with a toroidal angle $\phi_t = 19$ degrees, and

height from the midplane $z = +0.22$ m, respectively (Fig. 1 b). The distance between the

head section of the SLIP and last closed flux surface (LCFS) is about 17 cm. The distance

is insensitive to the Shafranov shift when the volume-averaged toroidal beta $<\beta>$ is less

than 2.0 % [23]. The SLIP installed on the outboard side of the LHD is designed to detect

co-going, transition, or trapped fast ions. The scintillator is comprised of ZnS (Ag) (P11),

which is deposited onto a ~10-μm-thick aluminum-coated quartz plate. The ranges of ρ

and χ that can be detected by the SLIP are 2–24 cm and 20–70 degrees. For an E of 180

keV, the energy resolution is $\Delta E/E \sim 30$ % at χ of 30 degrees and increases to 50 % at a

pitch angle of 60 degrees; the resolution in χ is 2.5 degrees at all E/χ ranges. In these

experiments, the value of ρ for a fast ion with $E\sim180$ keV is about 18 cm at $B_{SLIP} = 0.37$ T.

The scintillation light pattern on the screen was measured with a 4×4 photomultiplier

(PMT) array and an image-intensified complementary metal-oxide semiconductor

(CMOS) camera, simultaneously. Rapid changes of fast-ion losses were measured with

the PMT, with a time response up to 5 μs. On the other hand, an image-intensified CMOS camera with a frame rate up to 2,000 fps and a 352×352-pixel image was used for the measurement of the detailed E and χ distributions of the loss flux. Detailed information of the SLIP is available in Refs. [24, 25].

Mirnov coil arrays positioned on the inner surface of the vacuum vessel were used to observe TAE modes. Toroidal and poloidal arrays of the Mirnov coils (Fig. 1 c) [26] are present. Each array gives the toroidal mode number n or poloidal mode number m, respectively. All Mirnov coils in the toroidal array are placed on the top of the horizontally elongated section of the vacuum vessel. The TAE amplitude is measured using a Mirnov coil of a toroidal array placed at $R = 3.84$ m, $\phi_t = 18.0$ degrees, and $z= +0.64$ m, respectively (Fig. 1 b and c). The poloidal magnetic fluctuation amplitude b_θ at the position was nearly insensitive to the change in the Shafranov shift of the plasma because the poloidal magnetic field strength is nearly independent of the magnetic axis position.

Concerning fundamental plasma parameters, the electron temperature T_e and electron density n_e profiles were measured by Thomson scattering diagnostics [27]. The line-averaged density was measured with a multi-channel far-infrared laser interferometer [28].

3. TAE-induced losses in plasmas with small and large Shafranov shifts

Excitation of TAEs and observations of the TAE-induced fast-ion losses were attempted for two types of plasmas - those with small and large Shafranov shifts in the configuration of R_{ax_vac} =3.60 m at a B_t of 0.60 T. In these experiments, plasmas were produced and sustained using only NBI heating. The small and large Shafranov shifts were produced by varying the NBI power and/or n_e. The direction of B_t was CCW, as seen from the top. In this configuration, the two NBIs create co-going transiting fast ions. Note that the co-going ions in LHD circulate in the same direction as the helical coil current, increasing the rotational transform.

First, experiments were performed on plasmas with small Shafranov shifts. The position of the actual magnetic axis R_{mag} was shifted to 3.75 m due to the finite plasma pressure. A typical discharge waveform together with the magnetic fluctuation spectrogram is shown in Figure 2a). Two MHD modes are identified from magnetic fluctuation analysis: one is a TAE and the other is a resistive interchange mode (RIC). At around 60 kHz, a TAE was observed whose mode number m/n was identified as ~1/1 from toroidal and poloidal Mirnov arrays. The RIC observed at frequency of less than 10 kHz was excited by edge plasma pressure at the magnetic-hill region, having a structure

in which $m/n = 1/1$. The central electron temperature, T_{e0}, was 0.8 keV, $\langle n_e \rangle$ was

$0.9 \times 10^{19} m^{-3}$, $\langle \beta \rangle$ was 1.1 %, and the total absorbed NBI power was 7 MW. The profiles

of T_e and n_e are shown in Figure 2b). Finite T_e and n_e exist at $r/a=1$ because LHD plasmas

have a stochastic region outside the LCFS which consists of a magnetic field line with a

relatively long connection length. The scintillation image in the time-frame of

$t=4.400$–4.402 s captured by the camera is shown in Figure 3a). There are two loss

domains. Fast ions with passing orbits reach one domain having χ values of 35–40

degrees (Γ_{SLIP9}). On the other hand, fast ions with transition orbits reach the domain

having χ values of 50–60 degrees (Γ_{SLIP1}). Note that transition ions lie in the χ zone

between the passing and the helically trapped orbits, and have toroidal reflection points at

irregular intervals. Those orbits are stochastic with a large deviation from the flux surface.

Figure 3b) shows the time evolution of the magnetic fluctuation at the TAE frequencies

together with the loss fluxes measured by PMTs. The beam-ion losses Γ_{SLIP} having E/χ of

150–180 keV/35–40 degrees increase, and are synchronized with each TAE burst. On the

other hand, Γ_{SLIP} having E/χ of ~180 keV/50–60 degrees always appears, even in the

MHD-quiescent phase. The scaling of the increment of Γ_{SLIP} induced by TAE instabilities

($\Delta\Gamma_{SLIP}$) on the magnetic fluctuation amplitude of the TAE instability at the Mirnov coil

position (b_{TAE}) is shown in Fig. 4. $\Delta\Gamma_{SLIP}$ is evaluated as the increment of Γ_{SLIP} from that

just before the TAE burst. Note that $\Delta\Gamma_{SLIP}$ is normalized by the fast-ion content generated by co-injected NBs $P_{NBabsco}\ \tau_{se}$, because loss fluxes are thought to be proportional to the fast-ion content. Here, τ_{se} indicates the Spitzer slowing-down time of the fast ions through scattering on electrons. As seen from Fig. 4, $\Delta\Gamma_{SLIP}/P_{NBabsco}\ \tau_{se}$ increases nearly linearly with b_{TAE}/B_t when b_{TAE}/B_t is less than 4.0×10^{-4} and saturates above b_{TAE}/B_t of 4.0×10^{-4}. The scaling on b_{TAE}/B_t when this parameter is less than 4.0×10^{-4} in plasmas with small Shafranov shift (i.e., $R_{mag} = 3.75$ m) follows a convective type of scaling, as discussed in Refs. [13, 29] for the relatively small b_{TAE}/B_t regime.

Second, experiments were performed on a plasma with a large Shafranov shift (i.e., $R_{mag} = 3.86$ m). A typical waveform is shown in Figure 5a) and typical T_e and n_e profiles are shown in Fig. 5b). The main plasma parameters were as follows: T_{e0}, 0.8 keV; $<n_e>$, $1.2\times10^{19}\text{m}^{-3}$; $<\beta>$, 1.8 %; and P_{NBabs}, 8 MW. TAE and RIC were identified from magnetic fluctuation analysis as was done for the small-shift plasmas. The mode numbers m/n of TAE and RIC were ~1/1 and 1/1, respectively. Note that the TAE mode excited in this plasma is not exactly the same as that of the small-shift plasma. The same TAE mode was weakly excited at an early stage of the discharge, but it was damped due to the increase of the shift. A typical scintillation image in the time-frame of t=3.200–3.202 s measured by the camera is shown in Fig. 6a). Three primary loss domains can be

10

recognized. Fast ions with passing orbits reach one domain having χ values of 25-35 degrees (Γ_{SLIP13} and Γ_{SLIP14}). These losses were mainly induced by RIC, as described in Ref. 22. Fast ions with passing and transition orbits reach the domains having χ values of 35–45 degrees (Γ_{SLIP10}) and 45–55 degrees (Γ_{SLIP6}), respectively. Figure 6 b) shows the time evolution of magnetic fluctuation together with Γ_{SLIP}. Enhancement of losses was observed in the region of E/χ of 50–180 keV/35–45 degrees, and are synchronized with each TAE burst. The scaling of $\Delta\Gamma_{\text{SLIP}}/P_{\text{NBabsco}}\tau_{\text{se}}$ on $b_{\text{TAE}}/B_{\text{t}}$ is shown in Fig. 7. The normalized loss flux increases nearly quadratically with the $b_{\text{TAE}}/B_{\text{t}}$. Unlike the case of a small Shafranov shift, the TAE-induced loss is thought to follow a diffusive type of loss scaling in plasmas with an R_{mag} of 3.86 m [13, 29].

4. Setup for the Orbit-following model

Numerical simulations were carried out to understand the characteristics of TAE-induced beam-ion losses in LHD. Figure 8 is a flowchart of the present modeling. As shown in this figure, the simulation is mainly composed of two orbit-following models. The orbit in the plasma region is followed using the DELTA5D code including TAE fluctuations [30]. Note that DELTA5D is applicable to orbit-tracking inside the plasma. Actually, fast-ion orbits outside the plasma must be followed to simulate

TAE-induced loss measurement because the distance between the LCFS (~17 cm) and the

SLIP is larger than the transverse Larmor radius (~9 cm). Therefore, the Lorentz orbit

simulation (LORBIT) code is used to follow the Lorentz orbit outside the plasma in the

vacuum magnetic field. The orbit trajectories calculated by both codes are joined at the

LCFS to judge whether escaping fast ions can be detected by the SLIP. In the following

calculation, profiles of ion temperature and density are assumed to be equal to those of

electrons because electron temperature is relatively low in the electron density range and

$T_e \sim T_i$ was observed in similar discharge conditions.

The MHD equilibrium was reconstructed using the VMEC2000 code [31] in the

fixed-boundary mode. The pressure profile was given by the T_e, n_e, T_i, and n_i profiles. In

reconstructing the MHD equilibrium, the beam pressure was adjusted so that the

calculated R_{mag} should agree with the observed R_{mag}. The birth profile of beam ions is

calculated by the HFREYA code [32]. Although three tangential NB injectors were used

in the experiments, only two co-injected NBs are considered in this calculation, because

the SLIP is capable of detecting only co-going ions. The guiding-center orbit of each

beam ion in Boozer coordinates is followed using the DELTA5D code and magnetic

perturbations due to TAEs are taken into account. In order for validity of the

guiding-centre model, the mode frequency should be lower than cyclotron frequency, and

Larmor radius should be smaller than scale of the device [33]. The cyclotron frequency (~ 9 MHz) is much faster than the fluctuation frequency (70 kHz), implying that the gyration period is shorter than the variation time of the fluctuating fields. The conditions on the spatial scale can be separated into components parallel and perpendicular to magnetic field. The characteristic scale length parallel to toroidal magnetic field in an LHD plasma will approximately correspond to the toroidal width of the helical field ripple created by helical coils. The scale is $2\pi \times 3.9$ (major radius [m])/10 (number of field period) ~ 2.5 m which is much larger than the step size of fast ions ($v \times \Delta t = 5 \times 10^6$ [m/s] $\times 1 \times 10^{-9}$ [s] = 0.005 m). The characteristic scale length perpendicular to magnetic field line is the minor radius of plasma (0.6 m). The ratio of ρ_P (0.06 m for a typical beam ion having E of 180 keV, χ of 30 degrees, and using B=0.6 T) to the minor radius is $\rho_P/a \sim 0.1$. The ratio is thought to be small enough to simulate the loss scaling on fluctuation amplitude since the scale of the Larmor radius might not affect the scaling in this range of ρ_P/a. The paper by Fredrickson [34] shows that guiding center orbit simulations reproduce the neutron drop due to TAE instabilities in NSTX for $\rho_P/a \sim 0.25$. Although the NSTX results cannot be straightforwardly applied to LHD plasmas, the guiding center orbit simulations may give reasonable answers with regard to the parametric loss scalings, even if the absolute values of loss flux are not as accurate. The Coulomb collisions between beam ions and the

background plasma are taken into account in DELTA5D using the Monte Carlo method [35]. The TAE fluctuations were modeled as $\mathbf{b} = \nabla \times (\alpha \mathbf{B})$ where $\alpha = \dfrac{\nabla_{//}\phi}{i\omega B}$ on the assumption that the parallel electric field $E_{//}$=0 in the code. The electric field parallel to the magnetic field produced by $\dfrac{\partial \alpha}{\partial t}$ is not canceled in this simulation; the details are described later. The frequency sweeping of TAE is also taken into account; that is the frequency of the TAE is changed as a function of time [13]. Here, α represents a general function of the position, amplitude and frequency of the magnetic fluctuation, ϕ represents the electric potential, and ω represents the angular frequency of TAE. The profile of ϕ was calculated by the AE3D code [36]. Mode numbers of $n = 1$ and $m = -10$ to 10 were considered in the calculation, motivated by the fact that the TAE observed in the experiment has a structure with $m/n = \sim1/1$. A frequency sweeping rate of 20 kHz/s, similar to the experimental observation, was included in the simulation. The electric field parallel to the magnetic field produced by $\dfrac{\partial \alpha}{\partial t}$ is expected to be canceled due to the electric polarization potential and the rapid electron response as assumed in ideal MHD theory, but such effects are not included in this simulation. In the LHD experiments, the amplitude of the TAE mode was fairly large, and the electric field due to the polarization potential would not have had a crucial impact on the TAE-induced loss scaling in the large amplitude range, above a certain threshold. The DELTA5D code provides the

14

escape of fast ions as they exit the LCFS, including information on E and χ. Next, the

fast-ion orbits from the SLIP to the LCFS were calculated, based on the vacuum magnetic

field, using the LORBIT code. Here, magnetic perturbations in the vacuum field cause by

TAE instabilities were not considered. Note that the orbit was calculated from the SLIP to

the LCFS backwards in time in this calculation. This approach is efficient in finding the

orbits reaching the SLIP with respect to calculation time. The velocity at the SLIP

position can be determined from the structure of the front and rear apertures of the SLIP.

The velocity of the ions that can enter the SLIP is limited by the aperture structure as

shown in Fig. 9. We only considered one set of apertures because the counter-going orbits

tend to deviate from the flux surface toward the inboard side, and thus cannot reach the

SLIP. In order to find consistent lost-ion orbits from the plasma interior to the SLIP, the

exit points of fast ions on the LCFS together with E and χ obtained by DELTA5D code

were compared with those obtained by the LORBIT code. Here, we judged that the

particle reaches the SLIP if the following three criteria are fulfilled: (1) sqrt((R_{LORBIT} −

$R_{\text{DELTA5D}})^2$ + (z_{LORBIT} − $z_{\text{DELTA5D}})^2$) − ρ_{p} < 0.2 × ρ_{p}, and ϕ_{DELTA5D} − ϕ_{LORBIT} < 0.1 degrees;

(2) $|\chi_{\text{DELTA5D}}$ − $\chi_{\text{LORBIT}}|$ < 5 degrees; and (3) $|E_{\text{DELTA5D}}$ − $E_{\text{LORBIT}}|$ < 5 keV. The subscripts

indicate which code provided each parameter. This scheme is equivalent to the

calculation that follows the orbits from the LCFS to the SLIP, giving them random gyro

phases. We evaluated the effect of the threshold value in the above criterion on the results

of lost fast ions. It was confirmed that the results do not change significantly, even if the

above thresholds are reduced by 1/2.

In LHD plasmas, TAEs are excited during neutral beam injection when beam ions are

generated, slowed down, pitch angle scattered and lost outside the plasma. In order to

simulate appreciable slowing-down, the following method was adopted. The present

version of DELTA5D code does not include the source term, so that the velocity

distribution of fast ions before TAE excitation was simulated by a sum of the following

five distribution functions obtained using the DELTA5D code at $t = 0$ (just after the NBI

switch-on), and t $= \tau_{se}/5$, $2\tau_{se}/5$, $3\tau_{se}/5$, and $4\tau_{se}/5$, where $\tau_{se} = 5$ ms (Fig. 10). In Fig. 10,

the slowing down time looks longer than τ_{se} evaluated using $T_e = T_{e0}/2$. The birth profile of

fast ions is peaked around r/a~0.4, as shown in Fig. 11. Because the birth position

of ,most of the fast ions is at the position $R > R_{mag}$, orbits of these fast ions are shifted to the

smaller r/a region due to curvature and grad-**B** drifts. That is, these fast ions mostly stay

in the hot plasma region of $T_e > T_{e0}/2$, and the actual slowing down time in the simulation

is more than a factor of two different from τ_{se} estimated using $T_e = T_{e0}/2$. Nevertheless, the

fast ions have already slowed down to ~130 keV at $t = 4\tau_{se}/5$, which corresponds to

$v_{//}$~0.7v_A, well below the fundamental passing ion resonance condition of the TAE. That

is, most of the fast ions that can resonate with the TAE through the fundamental resonance are included in the sum of distribution functions to $t=4\tau_{se}/5$.

TAE fluctuations with a specified amplitude were included in DELTA5D for each velocity distribution, as shown in Fig. 10. The resultant loss fluxes were evaluated by summing up the loss fluxes calculated for the above five cases.

5. Comparison of the model calculation results with the SLIP data

Figure 11 shows the birth profile of fast ions calculated using the HFREYA code for a plasma with R_{mag} of 3.86 m. The resulting birth profiles of the NBs are relatively flat and, judging from the χ distribution, the beam ion orbits were dominated by co-going transit orbits ($\chi < 50$ degrees). A shear Alfvén spectra calculated using the STELGAP code [37] is shown in Fig. 12 a. Profiles of ϕ for the TAE calculated using the AE3D code in these experiments are shown in Fig. 12 b. In this calculation, a pure hydrogen plasma is assumed. The electric potential ϕ profile of the TAE in the plasma with R_{mag}~3.86 m was wider than that in the plasma with R_{mag}~3.75m, as seen from Fig. 12 b. Moreover, the peak position moved inward. Orbits of 5,120 particles are followed in this calculation. Both the TAE frequency and the resonance condition change in time. If the frequency sweeping is not included in the calculation, fast-ion losses do not increase with the

amplitude of the TAE. This suggests that the resonance condition is easily mis-matched

due to the narrow mode frequency. The TAE frequency sweep is essential in this analysis.

Figure 13 shows the footprint positions of fast ions on the LCFS; these ions have been

transported from the interior region of the plasma by TAEs. The exit positions of the fast

ions are concentrated on the upper side of the relatively weak magnetic field region. That

area corresponds to the valley between two helical winding coils. The reason why these

footprints deviate slightly to the upper side is due to the fact that the direction of the ion

grad-B drift is upward, since B_t is directed to be CCW. Though fast-ion losses increase

with the TAE amplitude at the TAE peak position b_{TAE0}, the above-mentioned footprint

points remain unchanged with the increase in b_{TAE0}. The increment of the total number of

fast ions transported to the LCFS from that obtained in the very low-amplitude case of

b_{TAE0}/B of 10^{-7} (Δ(total loss)) is shown as a function of b_{TAE0}/B in Fig. 14 a. No increase of

loss is observed in the case of b_{TAE0}/B less than 10^{-5}. The fast ions reaching the LCFS in

the case of b_{TAE0}/B from 10^{-7} to 10^{-5} correspond to classical first-orbit losses. We subtract

them because they are not TAE-induced losses. The scaling shows that the number of fast

ions increases linearly with the TAE fluctuation amplitude in the smaller-Shafranov-shift

plasma while it increases quadratically with TAE amplitude in the larger-shift plasma.

Figure 14 b shows the energy distribution of fast ions reaching the LCFS. Fast ions

fulfilling $v_{//} \sim v_A$ ($E > 140$ keV) are lost due to the effect of the TAE instability in the simulation. No additional loss is expected, even if we use the distribution functions obtained for longer times than the slowing down time, because the distribution functions shown in Fig.10 at $t=4\times\tau_{se}/5$ have already slowed down to ~130 keV. In order to investigate the impact of the finite ratio of ρ_h/a on the fast ion loss characteristics, a numerical test has been done with B_t artificially increased by a factor of 1.5. The scaling is then investigated as the value of ρ_p/a is lowered down to 0.06 from ~0.1. The enhanced B_t reduces the loss flux, but the scaling of the flux on b_{TAE}/B remains unchanged, as shown in Fig.14 c. It is thus concluded that the GC model employed in this simulation gives reliable results for the scaling of the flux on b_{TAE}/B.

In the LORBIT calculation, particles having energy from 120 keV to 200 keV in 10 keV steps are considered: 25,000 values of velocity are considered in each case according to the aperture structure of the SLIP. The start and end of the velocity vectors were decided using 0.5 mm × 0.5 mm grid points for each aperture. Figure 15 a) shows the E and χ distribution for the fast ions measured by the SLIP at an R_{mag} of 3.86 m. Figure 15 b) shows the calculated χ distribution of the fast ions reaching the SLIP. Note that the fast ions in the energy range from 120 keV to 180 keV are counted for each χ in Fig. 15 b). The loss flux having χ=35–45 degrees increases with the increase in b_{TAE0}/B

19

preferentially, as observed in the experiments. The loss flux $\Delta\Gamma_{SLIP}$ calculated by the model is shown as a function of b_{TAE0}/B in Fig. 16. It increases not only due to the increasing value of b_{TAE0}/B, but also due to that of the Shafranov shift. The scaling on b_{TAE0}/B obtained by the simulation agrees well with that observed in large Shafranov-shift plasmas. For small Shafranov-shift plasmas, the scaling on b_{TAE0}/B obtained by the simulation is noticeably stronger than that observed experimentally, which is shown in Fig.4. In this simulation, some of fast ions may be lost diffusively due to the relatively large amplitude of the TAE, since the TAE mode is not damped in this simulation. It may cause a steeper scaling of fast ion losses on the amplitude

Note that the fluctuation amplitudes b_{TAE} and b_{TAE0} cannot be directly compared since VMEC2000/AE3D only applies to the region inside the LCFS, so that the fluctuation amplitude at the Mirnov coil position is not evaluated from VMEC2000/AE3D. However, based on a crude cylindrical plasma assumption, the magnitude of the poloidal magnetic field inside the plasma, b_θ, is approximately expressed as (See Appendix)

$$b_\theta \approx -\frac{nB_z}{\omega R}\frac{\partial}{\partial r}\left[\phi\left(1-\frac{m}{n}\iota\big/2\pi\right)\right], \qquad (1)$$

using the electric potential calculated by AE3D. Here, θ, $\iota/2\pi$, r, and z represent poloidal direction, rotational transform, minor radius, and toroidal direction, respectively. The poloidal field in the vacuum region is expressed as [38]

$$\tilde{b}_\theta \square\ imAr^{-(m+1)}\left(1+\left(\frac{r}{b}\right)^{2m}\right),$$
(2)

where $b^{0/0}{}_\theta$, ω, i, ζ, A, and b represent the poloidal magnetic fluctuation, angular

frequency, imaginary unit, a longitudinal direction, amplitude of fluctuation, and the

conducting wall position, respectively. In the present experimental conditions, the

magnetic probe position corresponds to $r/a \sim 1.3$, and the TAE gap position is at $r/a \sim 0.7$,

where the distance from the magnetic probe to the TAE gap position is $\sim$32 cm. Using

equations (1) and (2), we can estimate the enhancement factors of the poloidal magnetic

fluctuation amplitude measured at the probe position in the gap position, for two cases

shown in Fig.12 (b). It is estimated to be $\sim$20 in the case of $R_{mag}\sim$3.75 m, and $\sim$15 in the

case of $R_{mag}\sim$3.86 m, respectively. Note that the magnetic probe detects dominantly the

Fourier component having the lowest poloidal mode number, i.e, $m=1$, and $m=1$ was

assumed in the above equations. Accordingly, the value of b_{TAE0} is expected to be roughly

proportional to b_{TAE} at the probe position.

The calculated scaling of $\Delta\Gamma_{SLIP}$ on b_{TAE0}/B is almost the same as that of Δ(total).

This suggests that the SLIP reflects the global nature of the escaping ions transported by

TAEs from the interior region to the LCFS. This fact also can be seen from Fig.17 a),

which shows the confinement and loss regions of fast ions on the LCFS. This calculation

result is obtained for fast ions having E=180 keV and χ=40 degrees, of which the ranges

of E and χ correspond to those typically detected by SLIP in the present experiments. If fast ions are in the "blue" region on the LCFS shown in Fig. 17 a), they always reach the SLIP without any losses in the trajectory of the orbit from the LCFS to the SLIP. If the fast ions are in the "white" region, they are always lost to the wall before reaching the SLIP. If the fast ions are in the "black" region, they are confined and never reach the SLIP. Actually, the DELTA5D simulation has suggested that the fast ions having E of ~180 keV and χ of ~40 degrees are transported by TAEs from the plasma interior to the positions on the LCFS indicated by red crosses. Most of these points are in the "blue" region, and should be detectable by the SLIP as lost ions. The loss scaling dependence exponent of 1 in the Δ(total loss) shown in Fig.14 is changed to 1.5 in the simulated SLIP signal $\Delta\Gamma_{SLIP}$. The detection rate of the SLIP as a function of velocity is not uniform because the velocity is decided by structure of aperture. The detection rate is thought to influence the changing of the loss scaling dependence. Figure 17 b) shows the confinement and loss regions on the LCFS for fast ions of E=180 keV having an appreciably large pitch angle χ of 66 degrees. Most of these fast ions cannot reach the SLIP and are not expected to be detected by the SLIP as lost fast ions.

6. Summary

Measurements of the energy (E) and pitch angle (χ) of lost fast ions induced by $m/n = {\sim}1/1$ TAE were carried out in two types of plasmas with smaller and larger Shafranov shifts for the LHD configuration with $R_{ax\_vac} = 3.60$ m. TAE-induced losses were observed in the range of $E/\chi \sim$50–180 keV/~40 degrees. The normalized loss flux increased as the TAE amplitude increased, as measured with a Mirnov coil placed outside the plasma. As the Shafranov shift increased, the TAE-induced losses increased and the scaling of the loss flux on the TAE amplitude became stronger. It seems that this tendency was due to the appreciable broadening of the TAE electric potentials and/or the expansion of the loss boundary due to large deviations of the orbit from the flux surface. Experimentally observed TAE-induced losses were simulated by the orbit-following model. The TAE-induced loss fluxes deduced by this model were concentrated around a particular range of χ that was nearly the same as that observed in the experiments. The loss fluxes increased with the increase in b_{TAE0}/B and/or R_{mag}. The loss scaling on the TAE amplitude became steeper as the Shafranov shift increased. The characteristics of the TAE-induced losses measured by the SLIP had the same tendency as the calculated characteristics of the fast ions transported by TAEs from the plasma interior to the LCFS, because most of the fast ions reaching the LCFS having a particular χ around 40 degrees could be detected by the SLIP in the LHD magnetic configurations.

Acknowledgements

Appendix

The magnetic fluctuation amplitude in an ideal MHD plasma is represented as:

$$b = \nabla \times \left[\xi \times B \right] \tag{A.1}$$

Here, b and ξ represent the magnetic fluctuation and displacement. In cylindrical coordinates (r, θ, z), the unit vector is set to $e_r = \nabla r$, $e_\theta = r\nabla\theta$ and $e_z = R\nabla z$, where e_j represents the unit vector in the j direction. I we assume $B = \left(0, B_\theta, B_z \right)$, $\xi = \left(\xi_r, \xi_\theta, \xi_z \right)$, then the poloidal magnetic fluctuation b_θ is derived as

$$b_\theta = \frac{\partial}{\partial z}\left(\xi_\theta B_z - \xi_z B_\theta \right) - \frac{\partial}{\partial r}\left(\xi_r B_\theta \right) \tag{A.2}$$

I the TAE is modeled as a shear Alfvén wave, then

$$\nabla \cdot \xi = \frac{1}{r}\frac{\partial}{\partial r}\left(r\xi_r \right) + \frac{1}{r}\frac{\partial}{\partial\theta}\xi_\theta + \frac{\partial}{\partial z}\xi_z = 0 \tag{A.3}$$

$$\xi_z = 0 \tag{A.4}$$

The perturbations are respectively assumed to vary as: $\xi, \phi \propto \exp\left[i\left(\omega t + m\theta - {nz}/{R} \right) \right]$, from equations (A.3) and (A.4)

$$\xi_\theta = \frac{1}{im}\frac{\partial}{\partial r}\left(r\xi_r \right) \tag{A.5}$$

is derived. From equations (A.2), (A.4) and (A.5), b_θ is expressed as:

$$b_\theta = \frac{nB_z}{mR}\frac{\partial}{\partial r}\left(r\xi_r \right) - \frac{\partial}{\partial r}\left(\xi_r B_\theta \right) \tag{A.6}$$

The displacement induced by TAE is approximately derived from the ϕ obtained from the AE3D code as:

$$\xi = \int v\,dt \approx -\int \frac{\nabla\phi \times B}{B^2}\,dt = -\frac{i}{\omega}\frac{\phi\left(k \times B \right)}{B^2} \tag{A.7},$$

where v and k represent the velocity and the wave number. Then, the radial displacement is:

$$\xi_r \sim i\frac{m\phi}{r\omega B_z} \tag{A.8}.$$

Hence, b_θ can be derived from equations (A.6) and (A.8) as

$$b_\theta \approx -\frac{nB_z}{\omega R}\frac{\partial}{\partial r}\left[\phi\left(1-\frac{m}{n}\,{}^{\iota}\!\!\big/\!{}_{2\pi}\right)\right] \qquad \text{(A.6),}$$

where we use ${}^{\iota}\!\!\big/\!{}_{2\pi} = \dfrac{B_\theta R}{B_z r}$.

References

[1] Chen C. Z. and Chance M. S., 1986 Phys. Fluids **29**, 3695

[2] Fasoli A., Gormenzano C., Berk H. K. *et al.*, Progress in the ITER Physics Basis Chapter 5: Physics of energetic ions 2007 Nucl. Fusion **47**, S264

[3] Wong K. L., Fonck R. J., Paul S. F., *et al.*, 1991 Phys. Rev. Lett. **66** 1874.

[4] Heidbrink W. W., Straite E. J., Doyle E., *et al.*,1991 Nucl. Fusion 31 1635

[5] Darrow D. S., 2008 Rev. Sci. Instrum. **79** 023502

[6] García-Muñoz M., Fahrbach H.U., and Zohm H., 2009 Rev. Sci. Instrum. **80** 053503

[7] Baeumel S., Werner A., Semler R., *et al.*, 2004 Rev. Sci. Instrum. **75** 3563

[8] Zweben S. J., Boivin R.L., Diesso M., *et al.*, 1990 Nucl. Fusion **30** 1551

[9] Darrow D. S., Herrmann H. W., Johnson D.W., et al., 1995 Rev. Sci. Instrum. **66** 476

[10] Darrow D. S., Zweben S. J. and Herrmann H. W., 1997 Fusion Eng. Des. **34-5** 53

[11] Zweben S. J., Bundy R. V., Darrow D. S., *et al.*, 2000 Nucl. Fusion **40** 91

[12] Van Zeeland M. A., Heidbrink W. W., Fisher R. K., *et al.*, 2011 Phys. Plasmas **18** 056114

[13] Sigmar D.J., Hus C.T., White R. *et al*, 1992 Phys. Fluids B **4** 6

[14] Todo Y., Berk H. L., and Breizman B. N. 2010 Nucl. Fusion **50** 084016

[15] Toi K., Ogawa K., Isobe M., *et al.*, 2011 Plasma Phys. Control. Fusion **53** 024008

[16] Kolesnichenko Y. I., Konies A., Lutsenko V. V., and Yakovenko Y. V., 2011 Plasma Phys. Control. Fusion **53** 024007

[17] Isobe M., Darrow D. S., Kondo T. *et al*., 1999 Rev. Sci. Instrum. **70** 827

[18] Werner A., Weller A., Darrow D. S. *et al*, 2001 Rev. Sci. Instrum. **72** 1 780

[19] Isobe M., Toi, K., Matsushita, H. *et al*., 2006 Nucl. Fusion **46** S918.

[20] Weller A., Anton M., Geiger J., et al., 2001 Phys. Plasmas **8** 931

[21] Osakabe M., Yamamoto S., Toi K., *et al*., 2006 Nucl. Fusion **46** S911

[22] Ogawa K., Isobe M., Toi K., *et al*., 2010 Nucl Fusion **50** 084005

[23] Suzuki Y., Watanabe K. Y., Funaba H., *et al*., 2009 Plasma Fus. Res. **4** 036

[24] Ogawa K., Isobe M. and Toi K., 2009 J. Plasma Fusion Res. Series **8** 655

[25] Ogawa K., Isobe M. and Toi K., 2008 Plasma Fusion Res. **3** S1082

[26] Sakakibara S., Yamada H. And LHD Experiment Group, 2010 Fusion Sci. Technol. **58** 471

[27] Narihara K., Funaba H., Minami T., *et al*., 2010 Fusion Sci. Tech. **58** 345

[28] Tokuzawa T., Ito Y., Okajima S., *et al*., 2010 Fusion Sci. Tech. **58** 352

[29] Heidbrink W.W., Doung H. H., Manson J. *et al*., 1993 Phys. Fluids B **5** 2176

[30] Spong D. A., Carlsson D. B., Batcjelor D. B., *et al*., 1999 Bull. Am. Phys. Soc. 44 215

[31] Hirshman S. P. and O. Betancourt, 1991 J. Comput. Phys. **96** 99

[32] Murakami S., Nakajima N., Okamoto M. *et al*., 1995 Trans. Fusion Technol. **27** 256

[33] Northrop T. G. 1961 Ann. physics **15** 79

[34] Fredrickson E. D. Crocker N. A., Bell R.E., *et al*., 2009 Phys. Plasma **16** 122505

[35] Boozer A. and Kuo-Petravic G., 1981 Phys. Fluids, **24** 851

[36] Spong D.A., D'Azevedo E. and Todo Y., 2010 Phys. Plasmas **17** 022106

[37] Spong D. A. Sanchez R. and Weller A. 2003 Phys. Plasmas **10** 3217

[38] Takechi M., Toi K. and CHS Group, 1999 Rev. Sci. Instrum. **70** 442

a)

NB1

NB2

SLIP

NB3

13.5 m

aperture

B

b)

Mirnov coil

1.0

0.0

-1.0

Vertical position [m]

2.0   3.0   4.0   5.0   6.0   7.0   8.0

Major radius [m]
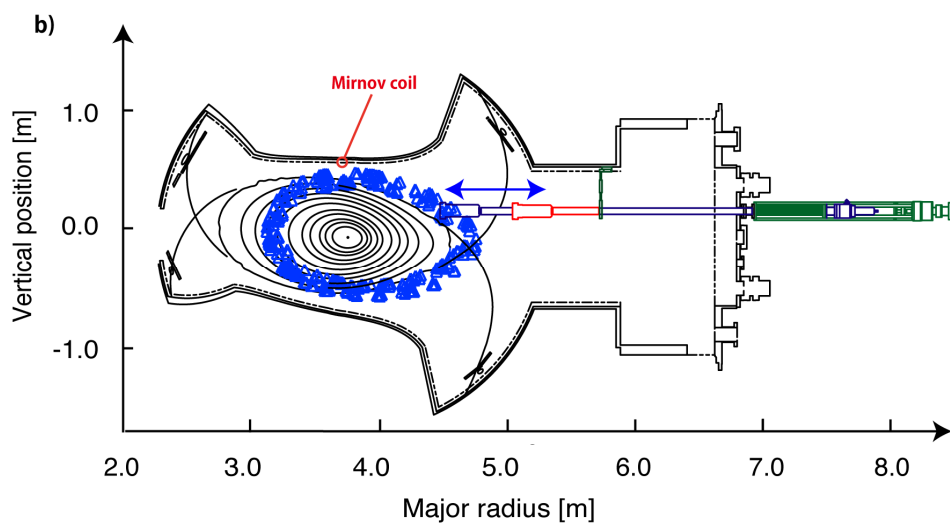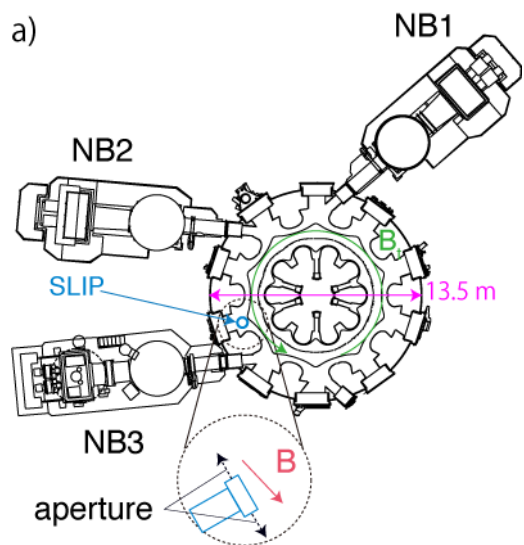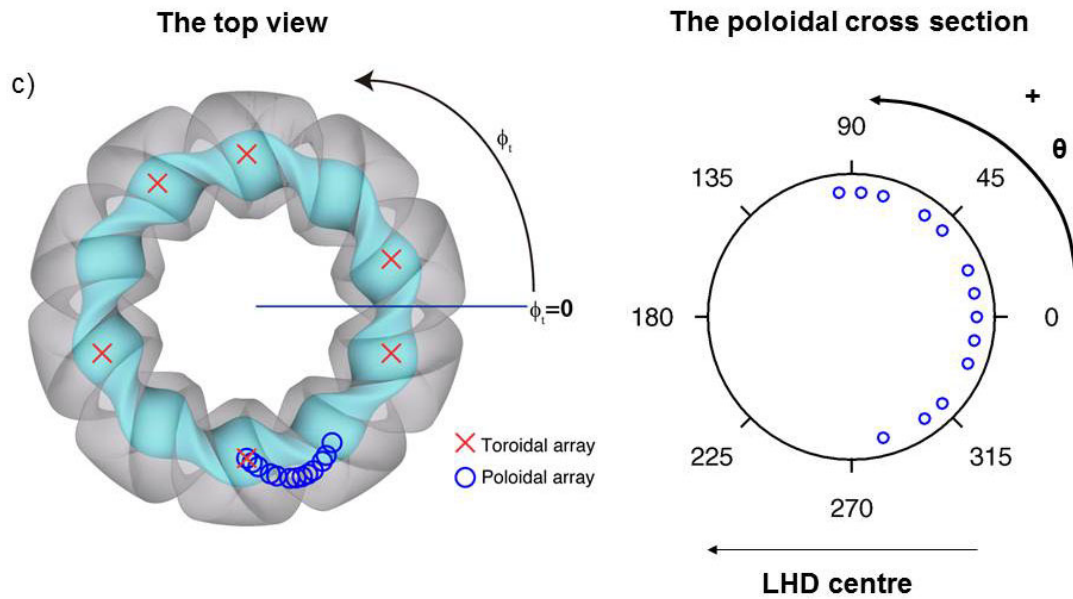
Fig. 1 a) A bird's-eye view of the LHD. The positions of the SLIP and three tangential NB injectors that provided super-Alfvénic ions are depicted. b) Schematic drawing of the SLIP installed on the outboard side of the LHD, the position of the Mirnov coil, and a Poincaré plot of the typical orbit that can be detected with the SLIP. The orbits of detectable ions deviated from magnetic flux surfaces. c) Positions of the Mirnov coil. The toroidal array consisted of six probes and the poloidal array consisted of thirteen probes.
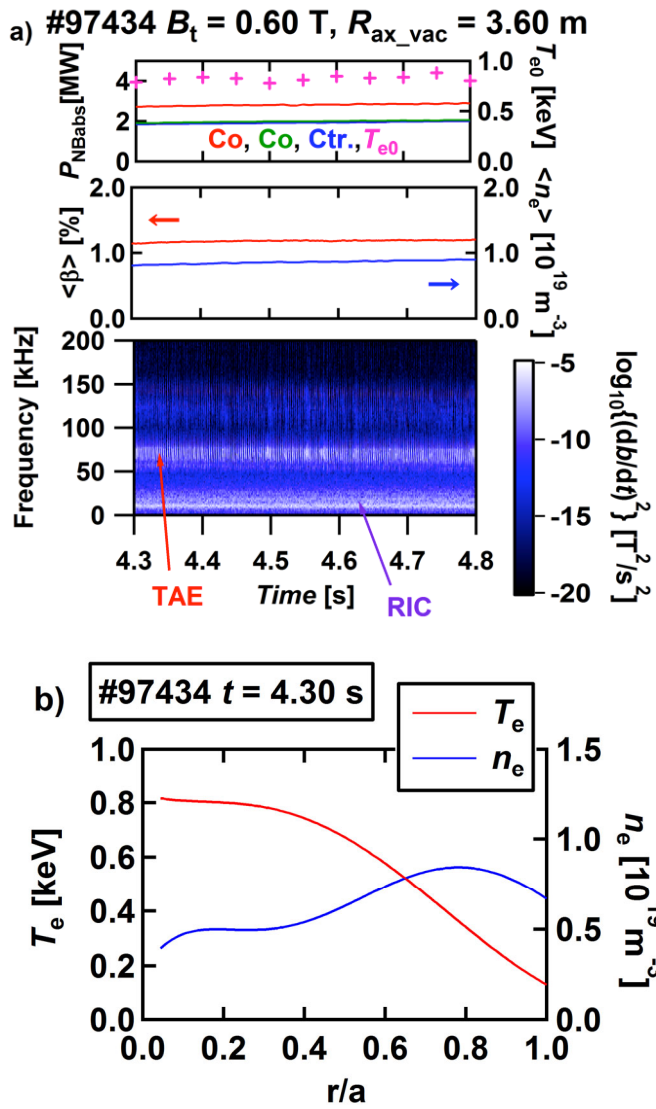
Fig. 2 a) Time evolution of NBI absorbed power, T_e, $<\beta>$, $<n_e>$ and a spectrogram of the Mirnov coil signal in small-Shafranov-shift plasma where TAE and RIC fluctuations were identified. b) Profiles of electron temperature and electron density at $t = 4.30$ s.
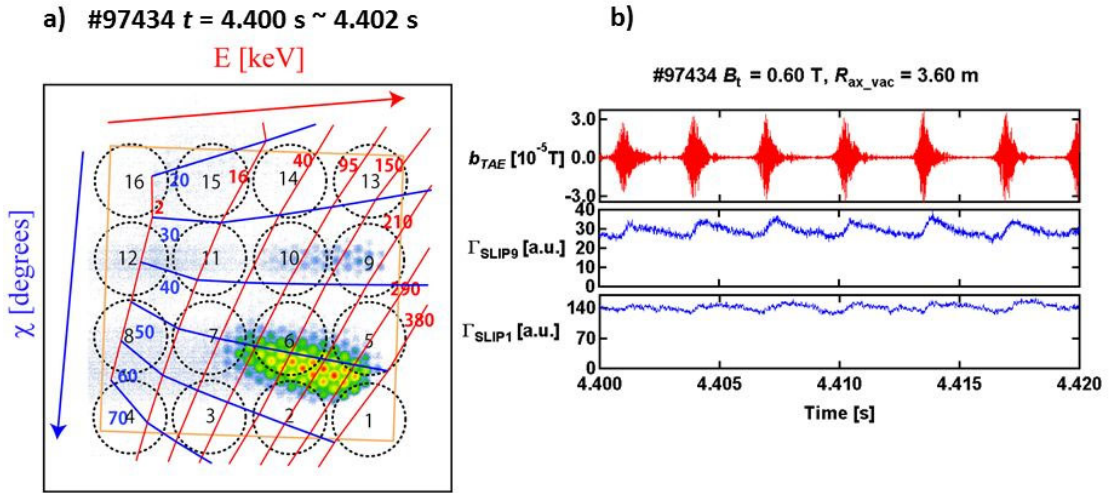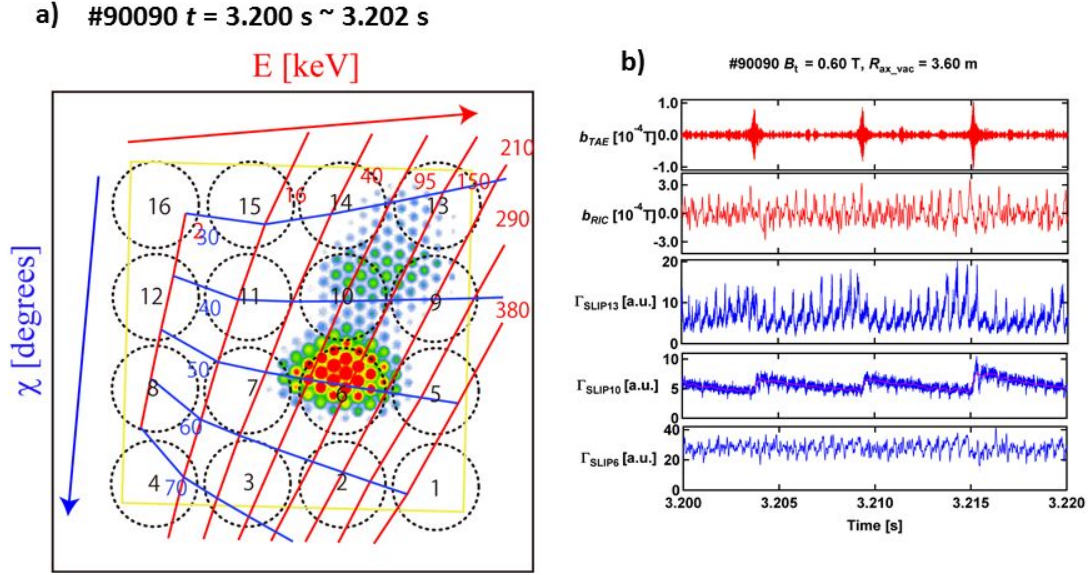
Fig. 3 a) Typical scintillation image captured by an image-intensified CMOS camera. Two dominant-loss domains can be recognized. The circles denote single-PMT observation regions. The value of ρ for a fast ion with $E \sim 180$ keV is about 18 cm. b) Time trace of magnetic fluctuation at the TAE range and two SLIP signals. TAE-induced loss is clearly observed in Γ_{SLIP9} (E/χ range of 130–180 keV/30–40 degrees). The signal in Γ_{SLIP1} (E/χ range of ~180 keV/50–60 degrees) is dominated by collisional loss.
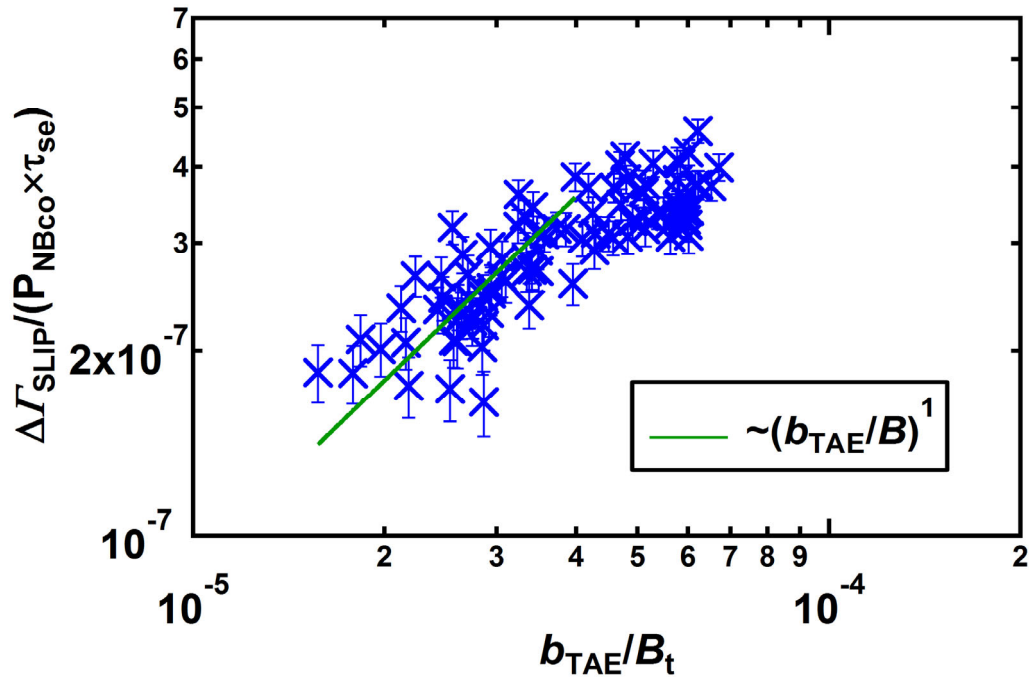
Fig. 4 Dependence of the increment of the loss flux induced by TAE on the magnetic fluctuation amplitude of TAEs. Error bars represent the white-noise level. The white noise in the loss flux signal Γ_{SLIP} was removed by the moving average technique.
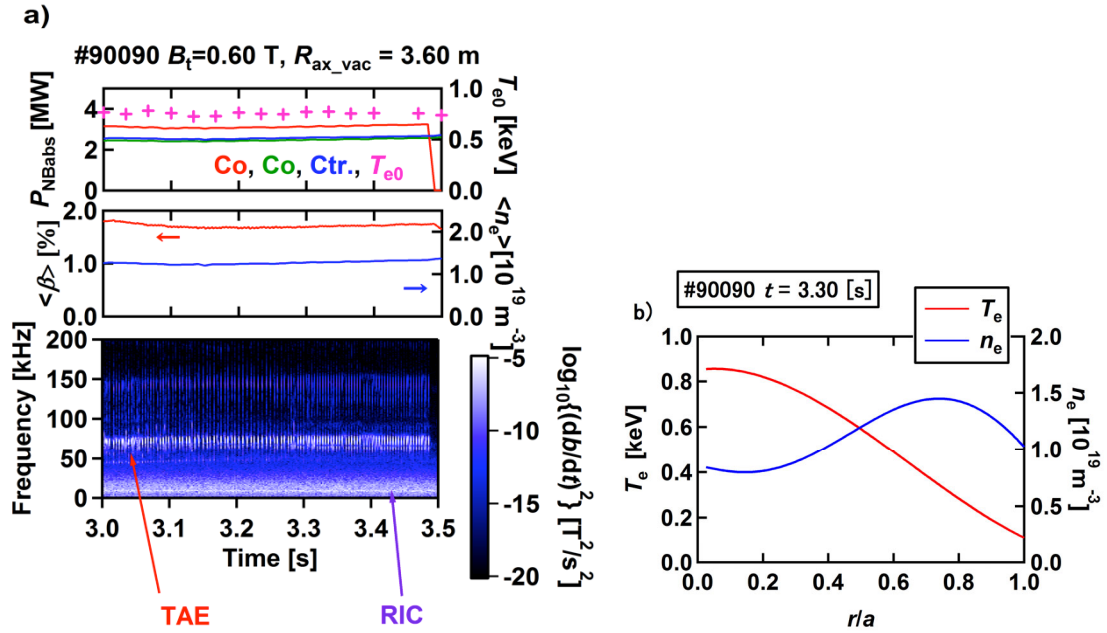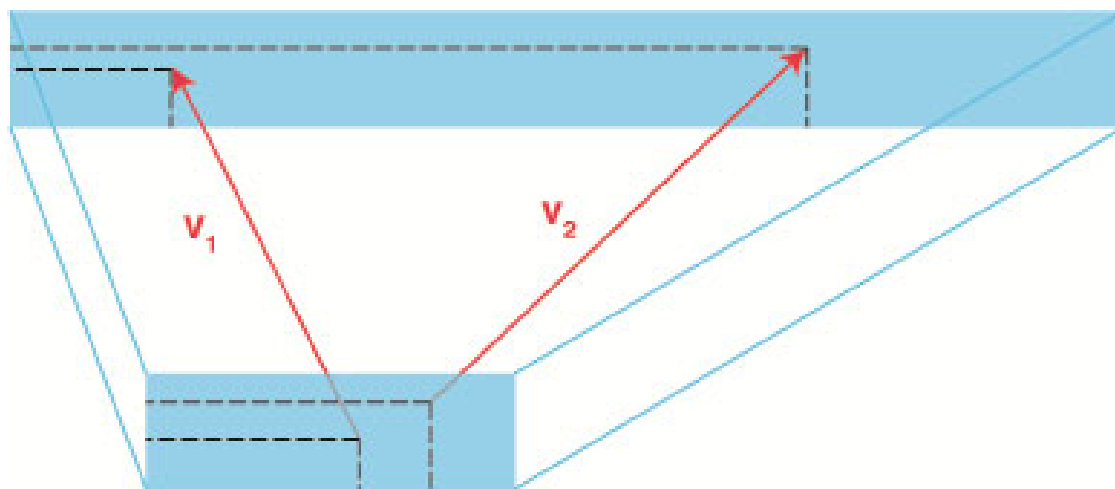
Fig. 5 a) Time evolution of NBI-absorbed power, T_e, $<\beta>$, $<n_e>$ and a spectrogram of the Mirnov coil signal in large-Shafranov-shift plasma where TAE and RIC fluctuations were identified. b) Profiles of electron temperature and the electron density at $t = 3.30$ s.

35

Fig. 6 a) Typical scintillation image captured by an image-intensified CMOS camera. There are three dominant-loss domains. The value of ρ for a fast ion with $E \sim 180$ keV is about 18 cm. b) Time trace of magnetic fluctuation at the TAE range and RIC range and the three SLIP signals. TAE-induced loss is clearly observed in Γ_{SLIP10} (E/χ range of 40–150 keV/35–45 degrees), RIC-induced loss is clearly observed in Γ_{SLIP13}(E/χ range of 100–180 keV/25–35 degrees) and collisional loss appear in Γ_{SLIP6} (E/χ range of 40–180 keV/45–60 degrees).
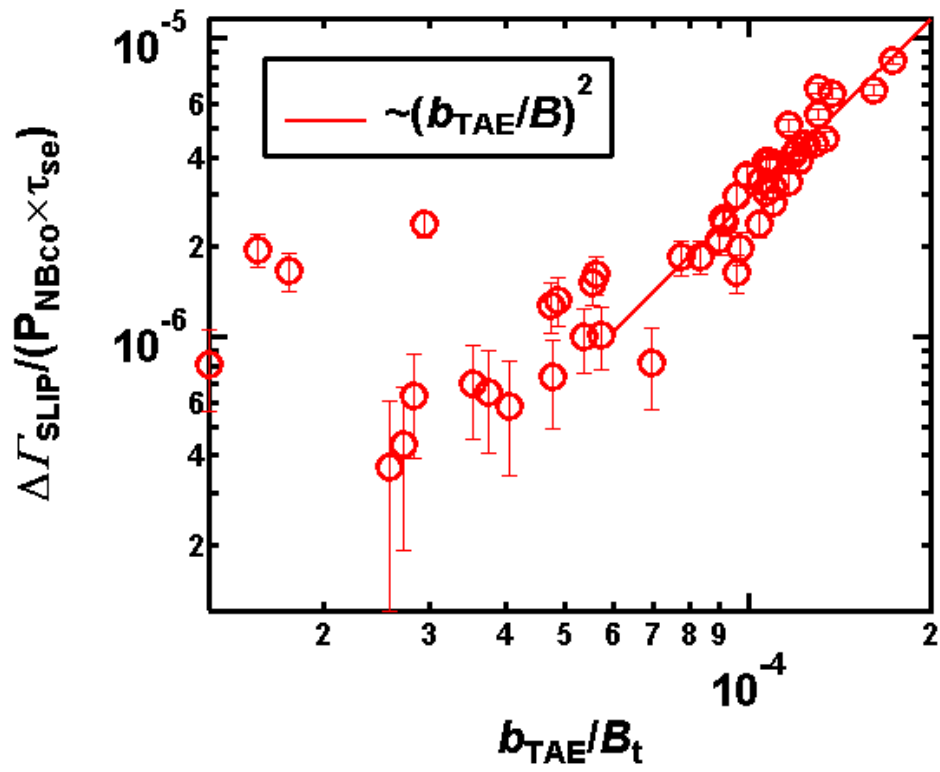
Fig. 7 Dependence of the increment of the loss flux induced by TAEs on the magnetic fluctuation amplitude of TAEs.
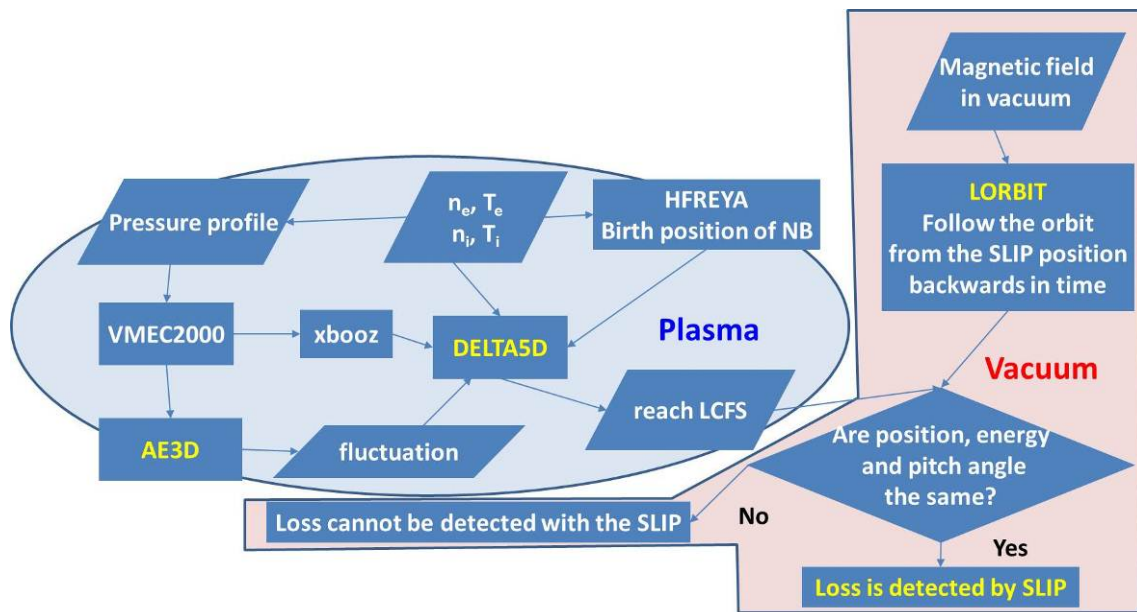
Fig. 8 Flowchart of the orbit-following models. Fast-ion orbits in the plasma are followed using the DELTA5D code, which takes into account TAE fluctuation. On the other hand, orbits outside the plasma are followed using the Lorentz orbit code.

Fig. 9 Model of apertures of the SLIP with the velocity of fast ions that can pass through

the aperture of the SLIP. The velocity is decided by two points located on the front and

rear apertures.
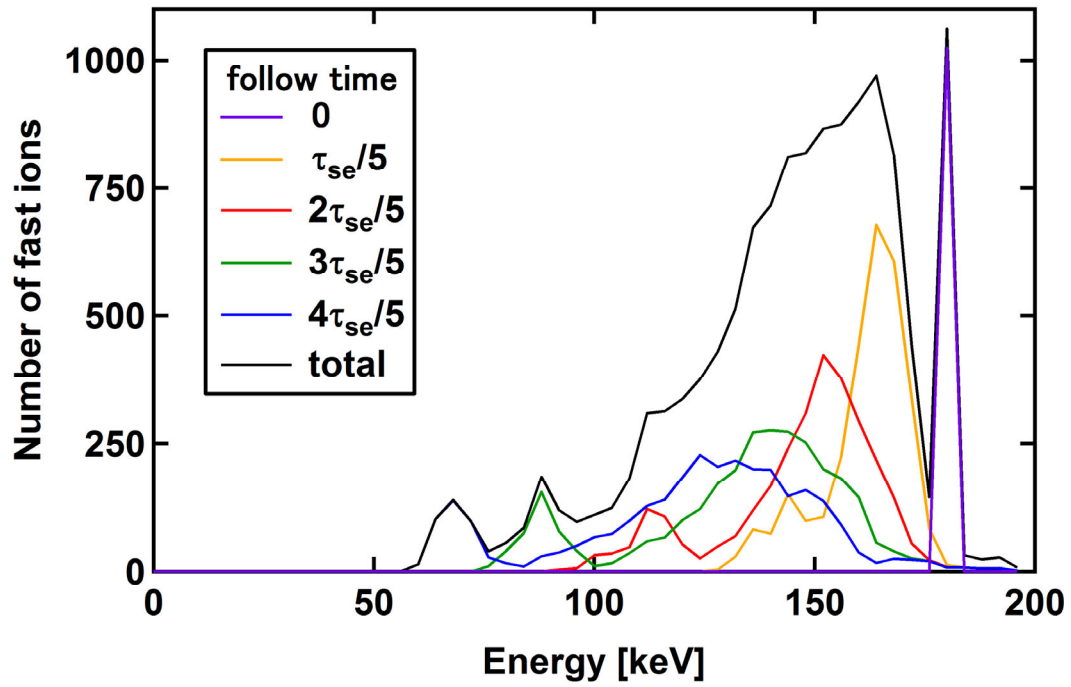
Fig. 10 Energy distributions of fast ions before TAE excitation calculated by DELTA5D

at $t = 0$ and $t = \tau_{se}/5$, $2\tau_{se}/5$, $3\tau_{se}/5$, and $4\tau_{se}/5$. Fast-ion distribution was modeled by

summing up the five cases.
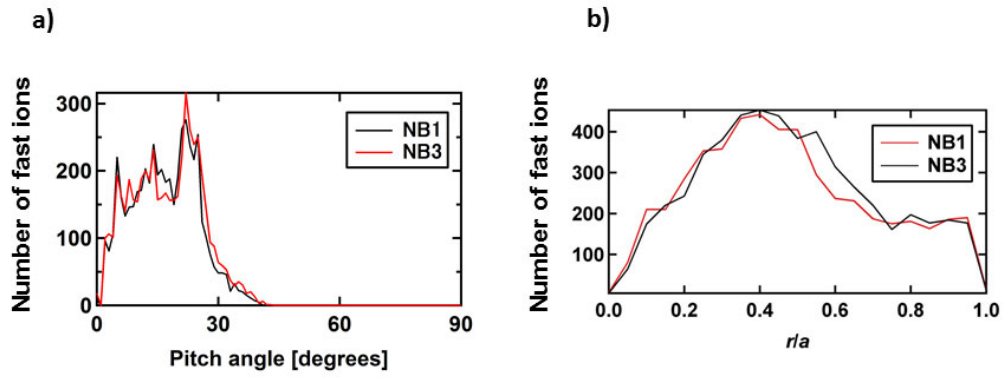
Fig. 11 Birth profiles of fast ions calculated by HFREYA in a plasma with R_{mag}=3.86 m. a)

Pitch-angle distributions of beam ions for co-injected NB1 and NB3. 5120 of beam

particles are considered on the calculation. b) Radial profiles of beam ions.
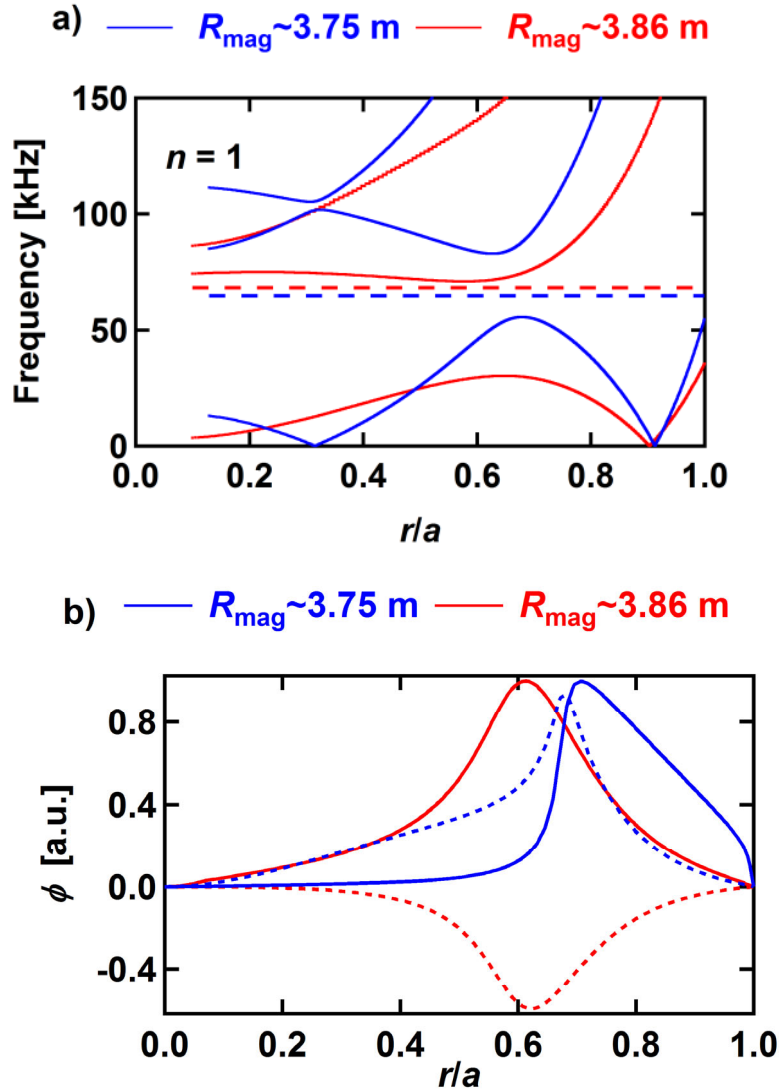
Fig. 12 a) Shear Alfvén spectra in the plasma with R_{mag} = 3.75 m (blue curve) and 3.86 m

(red curve) calculated by STELGAP code. b) Electric potential ϕ of TAE calculated by

AE3D code in the plasmas with R_{mag}=3.75 m (blue curves) and 3.86 m (red curves). Solid

lines and broken lines represent the $m/n = 1/1$ and $m/n = 2/1$ components of TAE,

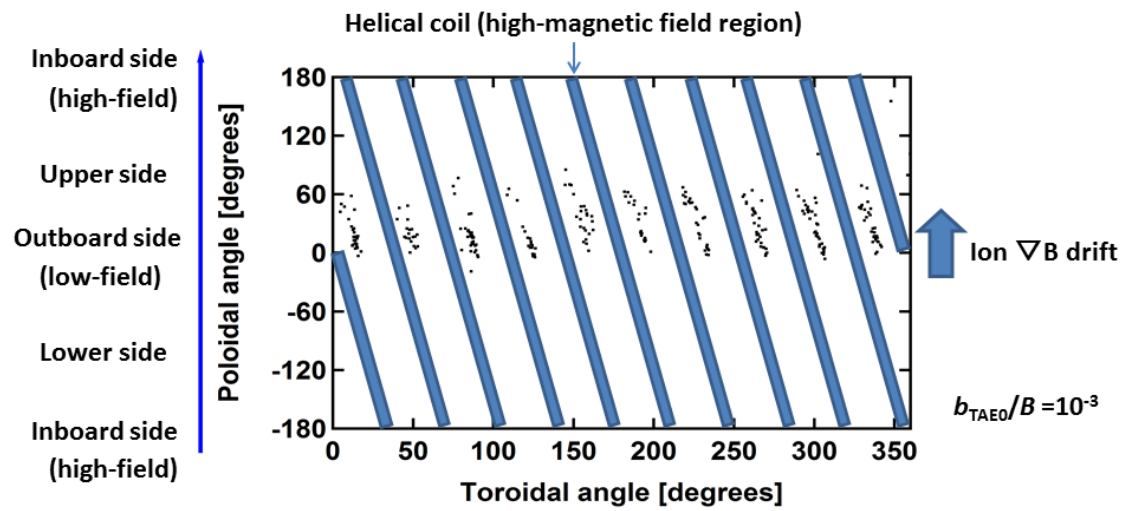respectively. The profile of ϕ becomes wider in the case of R_{mag} = 3.86 m.

Fig. 13 Exit points of the fast ions on the LCFS calculated by the DELTA5D code in the large-shift case. The thick blue lines show the high-magnetic field region where two-helical-coils were placed at such poloidal/toroidal angles.
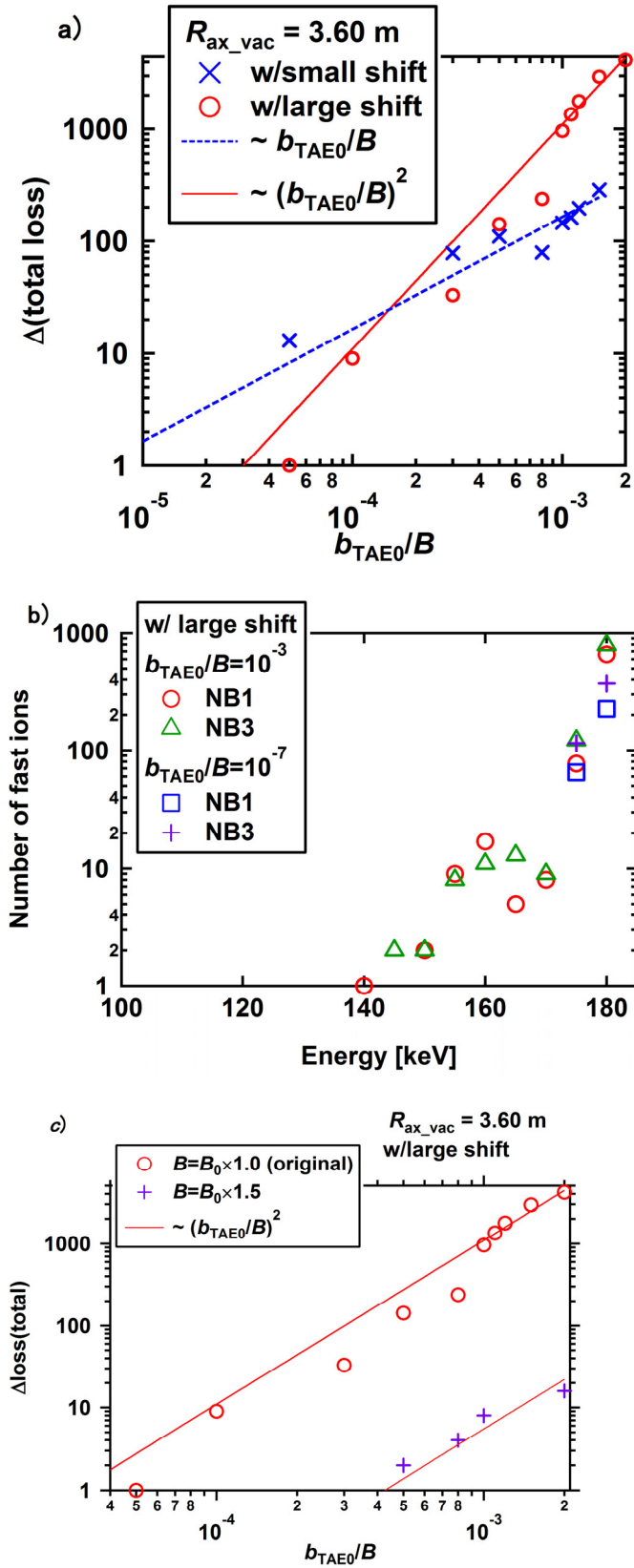
Fig. 14 a) The increment of the total number of fast ions reaching the LCFS as a function

of the TAE amplitude at the TAE gap position b_{TAE0} obtained using the DELTA5D code. The number of fast ions increases with the increase of the fluctuation amplitude and Shafranov shift. b) Energy distribution of fast ion loss in the case of no TAE and with TAE with a large shift plasma. No fast ions having E less than 140 keV are lost due to the TAE. c) The increment of the total number of fast ions reaching the LCFS as a function of b_{TAE0} using DELTA5D by artificially increased B_t by a factor of 1.5.
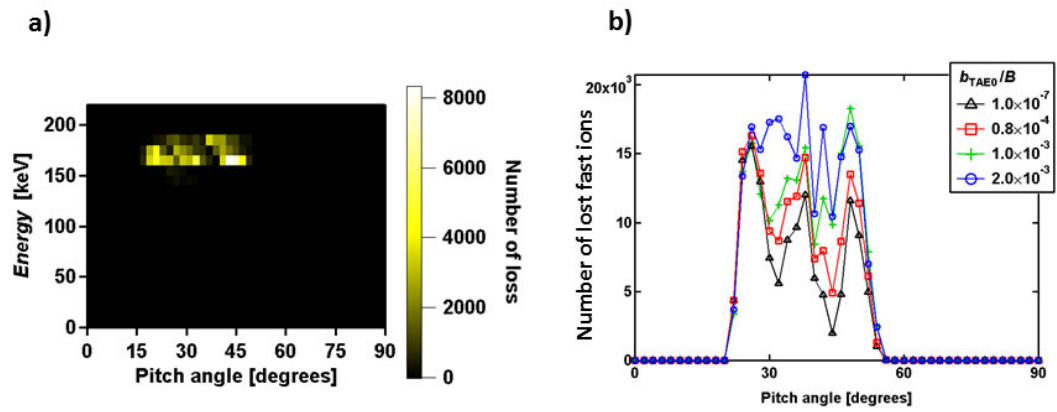
Fig. 15 a) Energy and pitch-angle distribution of escaping fast ions arrive at the SLIP in calculation. b) The calculated χ distribution of fast ions reaching the SLIP. There are three loss domains as obtained in the experiments.
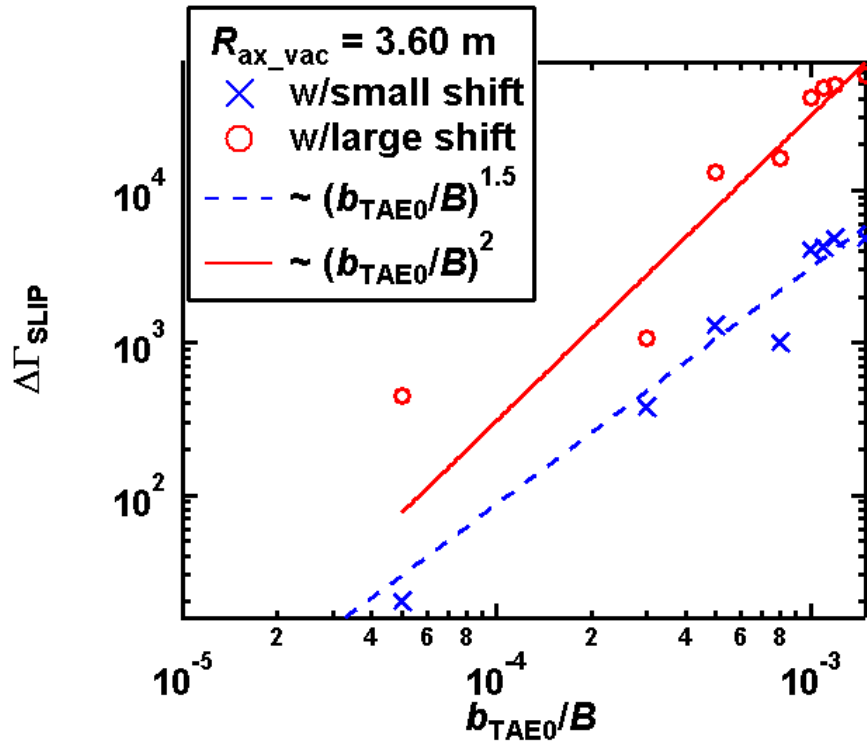
Fig. 16 Increment of fast-ion loss reaching the SLIP induced by the TAE as a function of

TAE-fluctuation amplitude at the TAE gap position b_{TAE0} in the calculation.
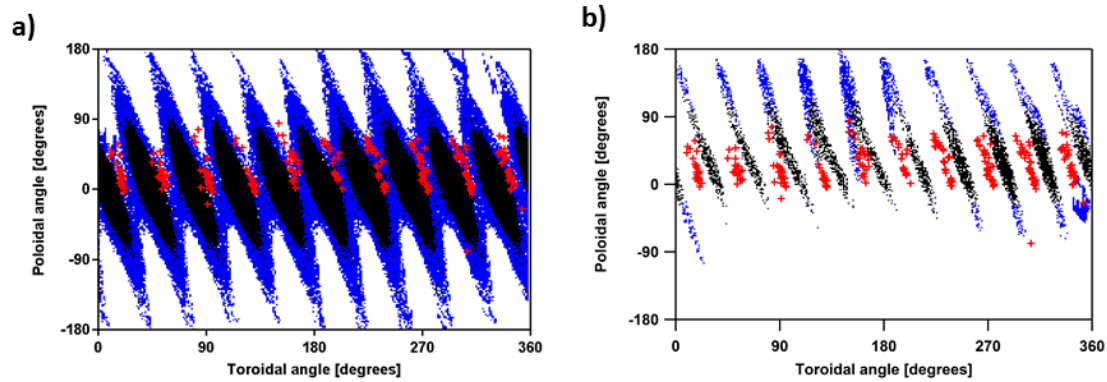
Fig. 17 The LCFS confinement and the loss regions obtained using the LORBIT code extended poloidally and toroidally. The white region corresponds to loss to the wall without detection by the SLIP. The blue region corresponds to fast ions reaching the SLIP. The black region corresponds to fast ions confined in the plasma region without reaching the SLIP. The position of exit points on LCFS of fast ions is indicated by red crosses. a) This evaluation was conducted for fast ions having an E/χ of 180 keV/ 40 degrees. b) This evaluation was conducted for fast ions having E/χ of 180 keV/ 66 degrees.